

Received April 8, 2020, accepted April 21, 2020, date of publication April 27, 2020, date of current version May 15, 2020.

Digital Object Identifier 10.1109/ACCESS.2020.2990494

# Dual Linearly-Polarized Antenna Array With High Gain and High Isolation for 5G Millimeter-Wave Applications

**BOTAO FENG**<sup>1</sup>, (Senior Member, IEEE), **YATING TU**<sup>1</sup>, **JUNLONG CHEN**<sup>1</sup>,  
**SIXING YIN**<sup>2</sup>, (Member, IEEE), AND **KWOK L. CHUNG**<sup>3</sup>, (Senior Member, IEEE)

<sup>1</sup>College of Electronics and Information Engineering, Shenzhen University, Shenzhen 518060, China

<sup>2</sup>Beijing Key Laboratory of Network System Architecture and Convergence, Beijing University of Posts and Telecommunications, Beijing 100876, China

<sup>3</sup>Civionics Research Laboratory, Qingdao University of Technology, Qingdao 266033, China

Corresponding author: Sixing Yin (yinsixing@bupt.edu.cn)

This work was supported in part by the International Cooperation Research Foundation of Shenzhen under Grant GJHZ20180418190621167, and in part by the Shenzhen Fundamental Research Foundation under Grant JCYJ20190808145013172.

**ABSTRACT** A dual linearly-polarized (LP) high-order-mode antenna with high gain and high isolation is proposed for 5G millimeter-wave (mm-wave) applications. To obtain high gain and wide bandwidth, a  $2 \times 2$  slot-fed magneto-electric (ME)-dipole antenna elements are excited by a high-order-mode  $TM_{430}$  cavity. Two substrate integrated waveguide (SIW) feeding networks that are vertically arranged in the bottom layers are employed to feed the high-order-mode cavity antenna for a double capacity, high isolation and low transmission loss. Moreover, an  $8 \times 8$  antenna array is fed by a pair of compact modified H-shaped full-corporate SIW networks. Measurement results show that an overlapped frequency bandwidth of 14.6% (36.8-42.6 GHz) with a peak gain of 25.8 dBi and an isolation of greater than 45 dB for the  $8 \times 8$  dual LP antenna array are achieved, which guarantee reliable high-speed data transmission and anti-interference capacity for 5G communications.

**INDEX TERMS** Dual polarized, high-order mode, 5G millimeter-wave applications, high gain, high isolation.

## I. INTRODUCTION

Millimeter-wave spectrum that spans very wide bandwidth has been officially allocated as one of frequency resources for the fifth generation (5G) mobile communications [1]. Among them, frequency bands of 37-42.5 GHz are relatively wider than other ones and hence are chosen as the high frequencies for mm-wave communications by Chinese Ministry of Industry and Information Technology [2]. As the stringent requirements such as high capacity, high-speed data transmission, and strong anti-interference ability need to be met for 5G communication system, where the antenna is a vital component that should be characterized by dual polarization, wide bandwidth, high gain and high isolation [3]. In addition, in order to be widely used in practice, antenna cost is a very important aspect in design consideration. Low-transmission-loss microstrip antenna with low cost is one of the most desirable options in mm-wave antenna design [4].

The associate editor coordinating the review of this manuscript and approving it for publication was Sudipta Chattopadhyay.

As is well known, mm-wave suffers from high atmosphere propagation loss that has severe impact on reliable data transmission. To address this problem, high gain in a wide bandwidth is desired for mm-wave antenna. A great number of high-performance designs have been proposed in the past years. A  $4 \times 4$  array composed of complementary ME-dipole antenna elements is excited by a low-loss T-junction SIW feeding network, a gain up to 19.6 dBi and a wide bandwidth of 22.6% can be simultaneously achieved [5]. Furthermore, a  $4 \times 4$  array composed of cross patch elements that are surrounded by rectangular cavities is fed by a slotted SIW network, a peak gain up to 21.4 dBi in the frequency bands of 56-63.1 GHz is realized in [6]. However, both of them only realize a single polarization, which cannot enhance the system capacity with a compact size. Instead of a metallic patch, a square dense dielectric patch antenna using frequency selective surface (FSS) superstrate layer is excited by an aperture-coupled feeding network [7]. High gain of 17.78 dBi at 28 GHz with a 9% bandwidth can be attained. Nevertheless, as there is a large air gap of about 5.4 mm

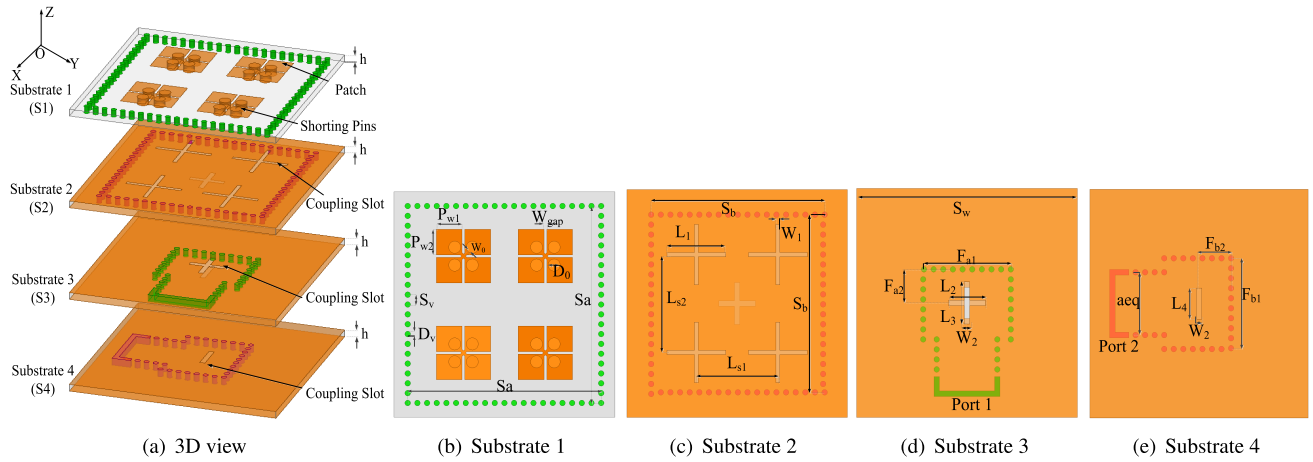


FIGURE 1. Geometry of the 2 × 2 dual linearly polarized antenna array.

between the radiating patch and the FSS superstrate layer, the antenna profile becomes high. In [8], bow-tie radiators are arranged to cross each other and fed by tilting feed-lines with 30°, resulting in high gain of 11.8-12.5 dBi over the frequency range of 57-64 GHz. Compared with conventional radiator, its radiating structure is relatively complicated. On the other hand, higher-order-mode cavity-backed antennas that they may yield wide bandwidth, high gain and high radiation efficiency without sacrificing size have drawn considerable interest in recent years [9]–[12]. Their outstanding characteristics demonstrate higher-order-mode cavity as an effective way to improve gain and other electrical performances.

In addition, isolation that indicates anti-interference ability is another key indicator for compact dual polarized mm-wave antennas. For this goal, several works with effective means were proposed recently. In [13], by etching U-shaped slots below a pair of vertically arranged feedlines, circulating current is yielded resulting in isolation up to 38.6 dB. By using an second bandgap in mushroom electromagnetic bandgap (EBG) structures, a high isolation of 40 dB can be achieved between transmitting and receiving microstrip array antennas [14]. A low-pass filter resonant cell is connected in series to the feedline for suppressing frequency signal [15]. Consequently, the channel isolation between the shared-aperture antennas reaches 65 dB. Among the above-mentioned typical methods, adopting filter structure and etching slots aside the feedlines may cause decrease of antenna gain, whereas there is a space limitation between the vertically arranged feedlines. Therefore, new means with high isolation are in urgent need for designing mm-wave antenna to cater for multiple high-performances.

As discussed above, the characteristics including high gain, high isolation across the whole wide bandwidth are the most important indicators for 5G mm-wave dual-polarized antenna. For achieving these goals, a dual LP high-order-mode mm-wave antenna with high gain and high isolation is proposed in this paper. Inspired by the ME-dipole antenna in [16], a high-order-mode cavity with TM<sub>430</sub> mode is employed

TABLE 1. Geometrical parameters of the 2 × 2 antenna subarray (Unit: mm).

Parameter	$F_{a1}$	$F_{a2}$	$F_{b1}$	$F_{b2}$	$L_1$	$L_2$	$L_3$	$L_4$
Value	6.36	2.3	6.3	2.35	4.26	2.66	2.95	2.18
Parameter	$L_{s1}$	$L_{s2}$	$P_{w1}$	$P_{w2}$	$S_a$	$S_b$	$W_0$	$W_1$
Value	5.92	6.88	1.86	1.8	14	12.5	0.2	0.3
Parameter	$W_2$	$a_{eq}$	$h$	$D_0$	$S_v$	$D_v$		
Value	0.4	4	0.787	0.86	0.7	0.4		

to excite a 2 × 2 slot-fed ME-dipole antenna subarray, resulting in high gain and wide bandwidth. Different from [16], the high-order-mode cavity is employed and fed by two vertically arranged slotted SIW feeding networks. By doing so, double capacity and high isolation are achieved without extra feeding networks. To further achieve high gain, an 8 × 8 antenna array fed by a pair of compact modified H-shaped full-corporate SIW networks is also proposed. Compared with the previously proposed dual-polarized mm-wave antennas, the proposed antenna array can achieve both high gain (25.8 dBi) and high isolation (45 dB) in a wide frequency band (36.8-42.6 GHz) by using a simple structure, which ensures the reliable high-speed data transmission and anti-interference capacity for 5G communications.

## II. DUAL LINEARLY POLARIZED ANTENNA

### A. 2 × 2 DUAL LINEARLY POLARIZED SUBARRAY ANTENNA

Fig. 1 and Table 1 show a detailed configuration of the proposed 2 × 2 dual LP subarray and its corresponding dimensions, respectively. To achieve high fabrication precision, the proposed antenna subarray is fully printed on four-layer Rogers RT/duroid 5880 substrates ( $\epsilon_r = 2.2$  and  $\tan\delta = 0.0009$ ) with each-layer thickness of 0.787 mm, as shown in Fig. 1(a). Two slotted SIW feeding networks are vertically arranged on the bottom layers (Substrate 3 and Substrate 4), respectively. Notably, a flat slot is etched in

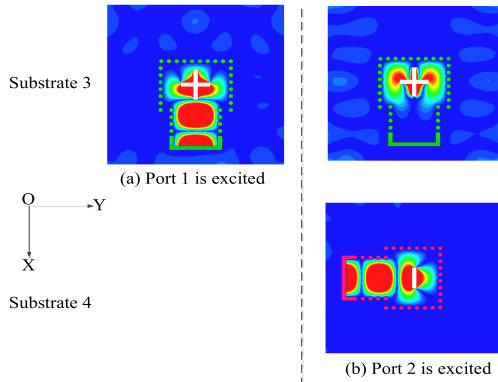


FIGURE 2. E-field distributions of the SIW feeding networks.

the center of the SIW on Substrate 4, while another cross slot is etched in the same place on Substrate 3. Thus, they independently couple signals to the upper layer cavity with high isolation. Here, the widths of short-end sections of the SIW in Substrate 4 change from  $a_{eq}$  to  $F_{b1}$ , which results in good impedance matching and determines the antenna resonant frequency range. The case is the same in Substrate 3. A high-order-mode resonant cavity etched with four cross-shaped slots is introduced in Substrate 2. In this way, the signal coupled from the bottom two slotted SIW networks is equally divided into four ways without extra feed network and increasing size. On the top substrate (Substrate 1), four complementary ME-dipole antenna elements are fed by the corresponding cross-shaped slots in the Substrate 3, respectively. Unlike the conventional dual LP ME-dipole antenna [17], there is a cross-shaped strip connecting the adjacent radiating electric dipoles whereas four metal columns are used to replace the shorted walls of the magnetic dipoles. In this case, good impedance matching as well as compact size can be realized by the proposed ME-dipole antenna element. In addition, due to the combination of the ME-dipole antenna and the cavity, high gain can be also stabilized in the desired frequency bands.

Fig. 2 displays the E-field distributions on SIW cavity feeding networks excited by Ports 1 and 2. As seen in Fig. 2(a), when Port 1 is excited, the horizontal part of the cross slot in Substrate 3 forces the E-field not to move forward, and hence the E-field intensity along its horizontal part becomes stronger. By contrast, as shown in Figs. 2(b) and 2(c), exciting Port 2 leads to stronger E-field intensity along the vertical flat slot in the SIW cavity in Substrate 4 and it goes over the vertical flat slot, whereas E-field distribution can be barely found on the horizontal part of the cross slot in Substrate 3. That is to say, the horizontal part of the cross slot in the Substrate 3 and the vertical flat slot in the Substrate 4 work independently, resulting in the very weak mutual coupling between the Ports 1 and 2.

To better understand how the high-order-mode cavity works, its E-field distributions for both ports at different frequencies are depicted in Fig. 3. As observed, they all operate

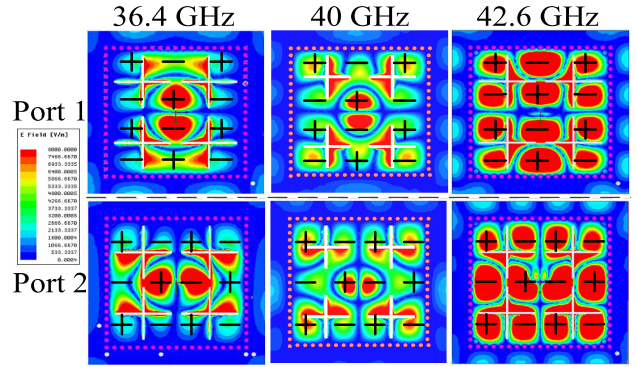


FIGURE 3. E-field distributions of the  $TE_{430}$  high order mode cavity.

with  $TE_{430}$  even though the electric field intensity changes as the frequency increases. For brevity, only the E-field distributions of Port 1 are discussed here. The E-fields on the neighbouring resonant points exhibit the same amplitude but the opposite phase. Notably, the direction of E-field is marked with “+” sign when the corresponding current flows towards the center of each resonant point. In contrast, it is marked with “-” sign when the corresponding current flows outwards the center of each resonant point. In our design, each dual LP antenna element is excited by one cross-shaped feeding slot, and it is expected that each antenna element is excited with same phases and amplitudes to obtain the uniform radiation. Because of the symmetric structure of the proposed dual LP ME-dipole element, the radiation directions of the four ME-dipole elements are always the same regardless of their arrangement. As a result, the high-order cavity can provide 4-way uniform excitations with high directional gain. In addition to that, low loss and compact size can be achieved as there is not any extra SIW network.

The initial cavity length (i.e.  $S_b$ ) can be calculated by the resonant frequency of the high-order-mode cavity ( $f_{mnp}$ ) as [18]:

$$\begin{cases} f_{mnp} = \frac{c_0}{2\sqrt{\epsilon_r}} \sqrt{\left(\frac{m}{a_{eq}}\right)^2 + \left(\frac{n}{b_{eq}}\right)^2 + \left(\frac{p}{c_{eq}}\right)^2} \\ a_{eq} = S_{b1} - 1.08 \frac{d_v^2}{S_v} + 0.1 \frac{d_v^2}{S_{b1}} \\ b_{eq} = S_{b2} - 1.08 \frac{d_v^2}{S_v} + 0.1 \frac{d_v^2}{S_{b2}} \end{cases} \quad (1)$$

where  $\epsilon_r$  is the permittivity of the substrate,  $m$ ,  $n$  and  $p$  stand for the numbers of variations in the standing wave pattern along the  $x$ -,  $y$ -, and  $z$ -axis directions, and  $a_{eq}$ ,  $b_{eq}$ , and  $c_{eq}$  represent the length, width and height of the equivalent resonant cavity, respectively. In addition, parameters  $d_v$  and  $S_v$  are the diameter of metallic vias and distance between the adjacent vias, respectively. In our case,  $m = 4$ ,  $n = 3$ ,  $p = 0$ ,  $S_b = S_{b1} = S_{b2}$ , and the resonant frequency  $f_{430}$  is selected for 39.5 GHz (center resonant frequency of the desired frequency band). Combined with the above factors, the calculated initial length of the cavity  $S_b$  is equal to 14 mm.

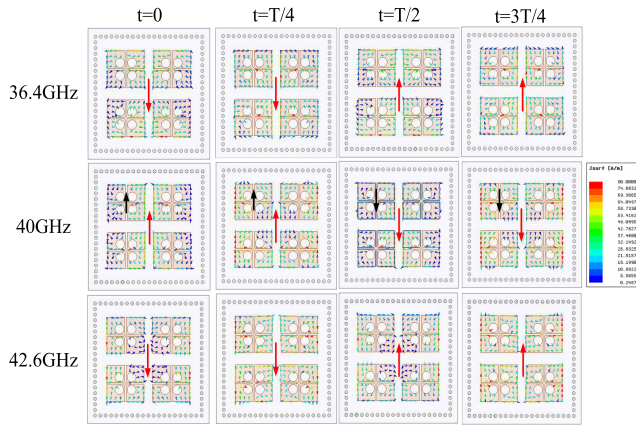
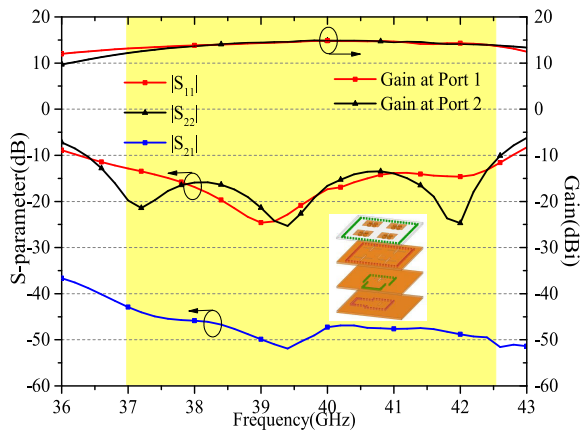
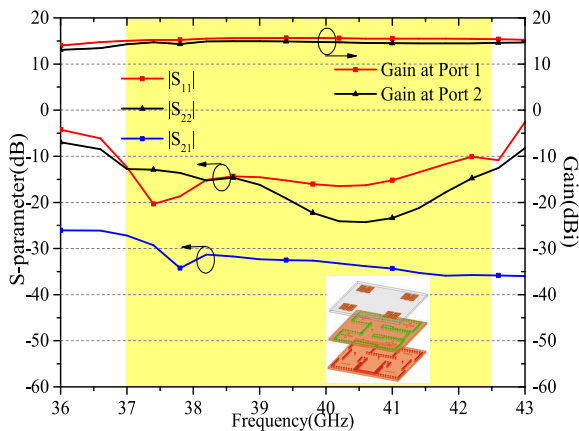


FIGURE 4. Current distributions on the 2 × 2 dual LP ME-dipole antenna subarray in the high-order-mode cavity for Port 1.



(a) Proposed antenna subarray



(b) Compared antenna subarray fed by H-shaped networks

FIGURE 5. Simulated S-parameters and gains of the proposed 2 × 2 dual LP antenna subarray and compared antenna subarray.

Fig. 4 shows the current distributions on the 2 × 2 ME-dipole antenna subarray in the high-order-mode cavity for Port 1. At the lower frequency of 36.4 GHz, the total currents for subarray (in red) mainly flow along the downward direction at both  $t = 0$  and  $t = T/4$ , then they redirect upward

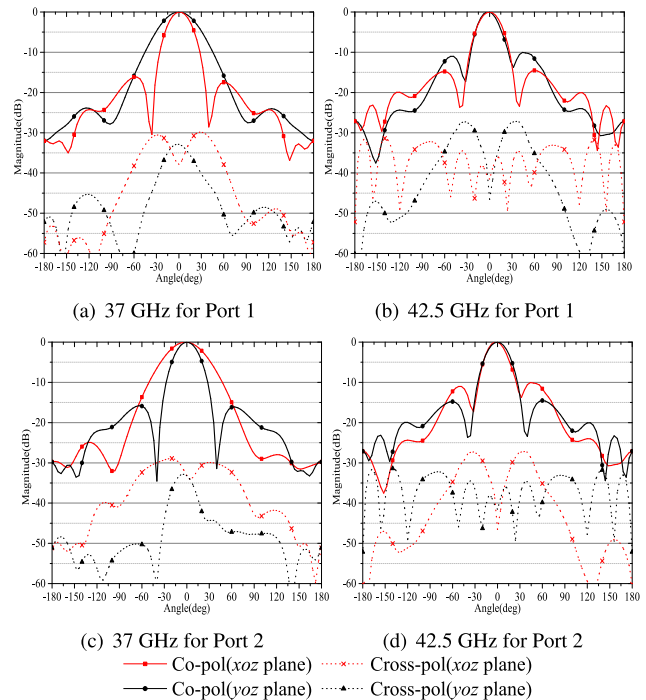


FIGURE 6. Simulated radiation patterns of the 2 × 2 dual LP antenna subarray at 37 and 42.5 GHz for both ports.

TABLE 2. Simulated radiation performance of the 2 × 2 dual LP antenna subarray at different frequencies.

Parameter	Port 1					
	XOZ-plane			YOZ-plane		
Frequency (GHz)	HPBW (deg)	X-pol (dB)	FBR (dB)	HPBW (deg)	X-pol (dB)	FBR (dB)
37	36	-29.8	32	48	-32.8	32
42.5	28.8	-28	26.1	28.4	-36.1	26.1
Port 2						
37	48	-28.8	29.7	33	-33.1	29
42.5	26	-27.2	27.1	28	-33.1	27.1

at both  $t = T/2$  and  $t = 3T/4$ . The current directions at 40 GHz are opposite to the ones at 36.4 GHz, whereas the current directions at 42.6 GHz are the same to that at 36.4 GHz. In other words, Port 1 excites the vertical linear polarization. Due to the symmetry, the condition of Port 2 is similar to that of Port 1 and it excites the horizontal linear polarization. In order to analyze the working principle of the high gain caused by ME dipole, the current distributions on the upper-left-corner ME dipole antenna element at 40 GHz are also plotted (in black). As observed, the current directions on the ME dipole antenna are the same to the antenna subarray. Notably, the current intensity is weak at  $t = 0$  and then enhances at  $t = T/4$ . Similarly, the current intensity becomes weak at  $t = T/2$ , and it enhances again at  $t = 3T/4$ . It can be inferred that the electric dipole and the magnetic dipole work in turn, resulting in complementary radiation pattern with high gain.



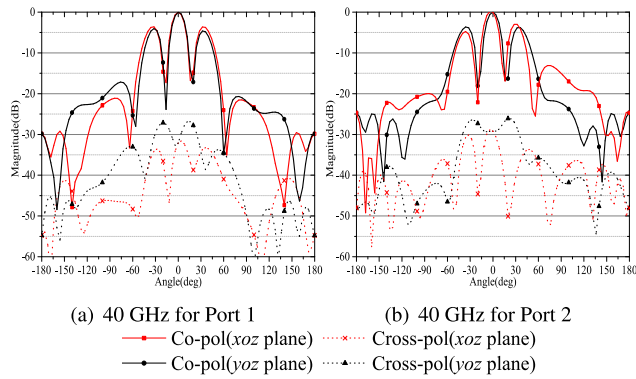


FIGURE 7. Simulated radiation patterns of the 2 × 2 dual LP antenna subarray with H-shaped feeding networks at 40 GHz for both ports.

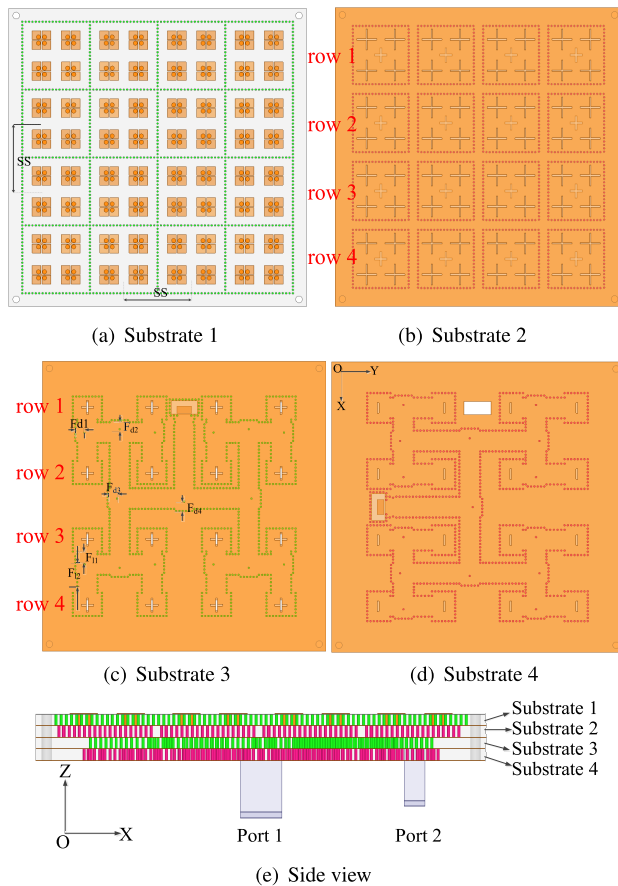


FIGURE 8. Geometry of the 8 × 8 dual linearly polarized antenna array.

TABLE 3. Geometrical parameters of the 8 × 8 antenna array (Unit: mm).

Parameter	$SS$	$F_{d1}$	$F_{d2}$	$F_{d3}$	$F_{d4}$	$F_{l1}$	$F_{l2}$	$F_m$
Value	14	2	1.92	2.05	2.02	3.01	6.26	0.43
Parameter	$L_{r1}$	$L_{r2}$	$W_{r1}$	$W_{r2}$	$W_{r3}$	$S_v$	$D_v$	$m_1$
Value	1.45	0.2	3.18	3	6.3	0.7	0.4	0.2

Fig. 5 shows the simulated S-parameters and gains of the proposed 2 × 2 dual LP antenna subarray and compared antenna subarray, which are the key performances for dual LP antennas. As shown in Fig. 5(a), the proposed overlapped

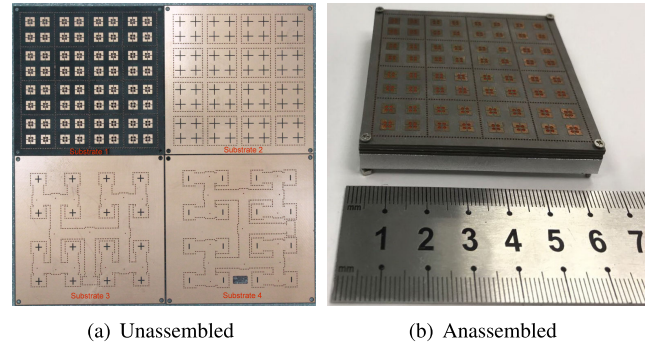


FIGURE 9. Photographs of the 8 × 8 LP antenna array prototype.

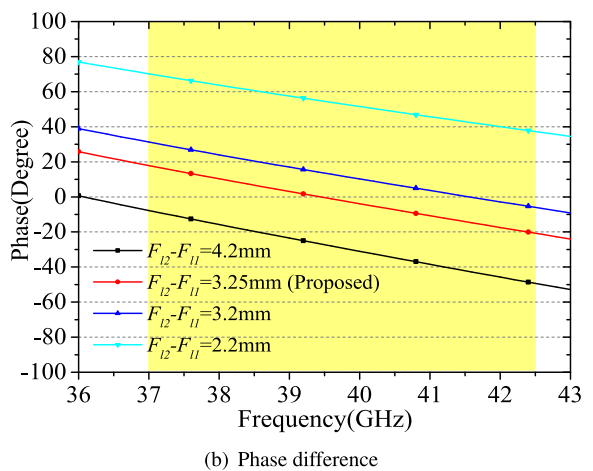
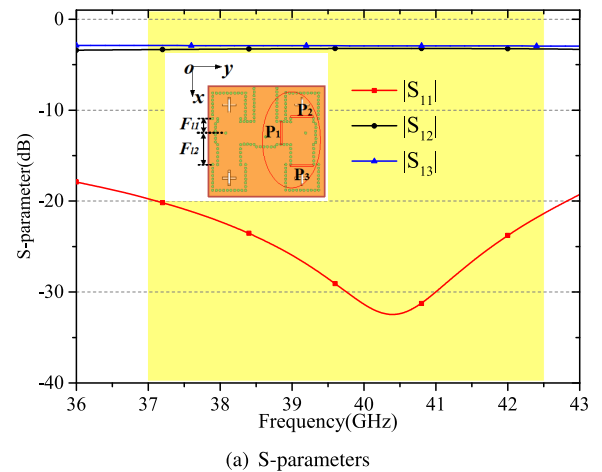


FIGURE 10. Performance of the T-junction of the H-shaped power divider.

impedance bandwidth between both ports ( $|S_{11}| \leq -10$  and  $|S_{22}| \leq -10$ ) is 15.7% from 36.4 GHz to 42.6 GHz with corresponding gain of  $13.29 \pm 1.59$  dBi. The bandwidth can cover the desired frequency band (37-42.5 GHz, in yellow color) and the gain is relatively stable. In addition,  $|S_{21}|$  is below  $-43$  dB across the desired frequency band, indicating low mutual coupling between both ports. As shown in Fig. 5(b), a conventional 2 × 2 dual LP antenna subarray fed by H-shaped networks is used for comparison. As seen,

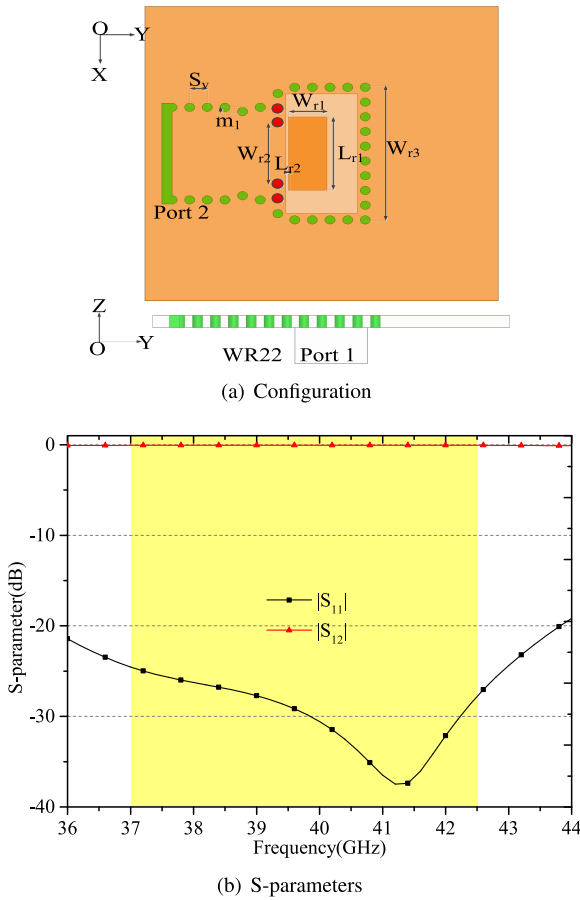


FIGURE 11. Performance of the metallic waveguide to SIW transition.

there is hardly any change in the compared gains, whereas the overlapped impedance bandwidth between both ports becomes slightly narrow and the  $|S_{21}|$  gets obviously worse ( $\leq -26$  dB). In other words, the high gain is mainly yielded by the ME-dipole antenna due to its complementary characteristics, whereas the impedance bandwidth is enhanced by the high-order mode cavity.

The corresponding radiation patterns and characteristics at 37 GHz and 42.5 GHz for both ports are exhibited in Fig. 6 and Table 2, respectively. For port 1 at 37 GHz, the half power beam width (HPBW), cross polarization level (X-pol), front-to-back ratio (FBR) are  $36^\circ$ ,  $-29.8$  dB and 32 dB, respectively, in XOZ-plane, while they are  $48^\circ$ ,  $-32.8$  dB and 32 dB, respectively, in YOZ-plane. At the upper frequency of 42.5 GHz, they are  $28.8^\circ$ ,  $-28$  dB and 26.1 dB, respectively, in XOZ-plane, and  $28.4^\circ$ ,  $-36.1$  dB and 26.1 dB, respectively, in YOZ-plane. In general, they exhibit low X-pol level and high FBR. The HPBWs are not excessively narrow owing to the relatively small number of antenna elements. They are nearly the mirror images between both ports due to the symmetric structure. In order to obtain good impedance bandwidth, the horizontal and vertical gap widths of the  $2 \times 2$  antenna array are unequal. Consequently, the radiation patterns are not exactly the same in the XOZ- and YOZ- planes

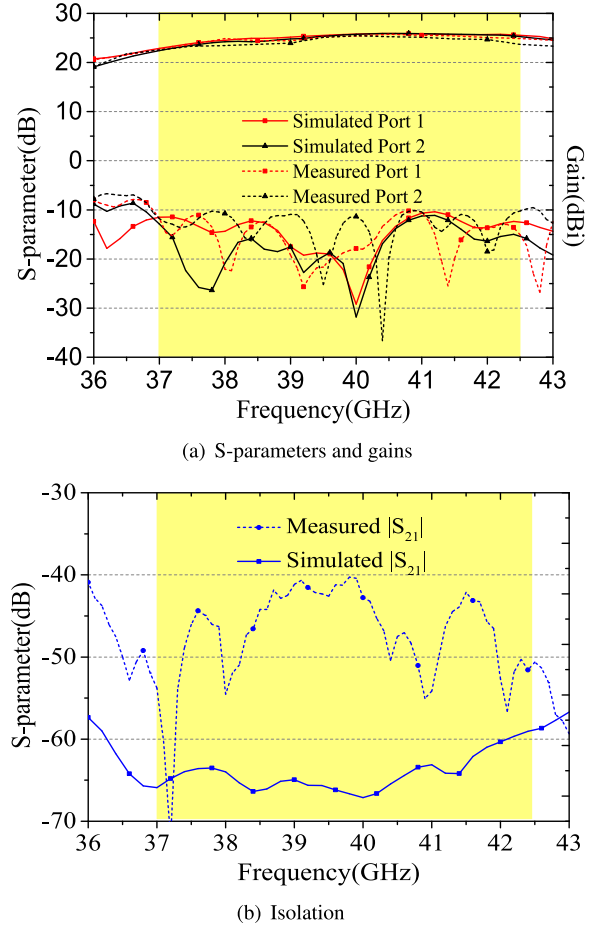


FIGURE 12. Performance of the  $8 \times 8$  dual LP antenna array.

for both ports. As shown in Fig. 6, at the lower frequency of 37 GHz, the HPBW in XOZ-plane of Port 1 is similar to the one in YOZ-plane of Port 2, while the HPBW in YOZ-plane of Port 1 is similar to the one in XOZ-plane of Port 2. Notably, the HPBWs in XOZ-plane and YOZ-plane of the same port are different. As the frequency increases, the HPBWs in both planes of the two ports become narrow and they have nearly the same values.

In comparison, Fig. 7 shows the radiation patterns of the compared antenna subarray fed by H-shaped networks. Because the coupling slots of H-shaped network are arranged in the four corners, the gap widths between the four ME-dipole antenna elements become large. Consequently, the side lobe level gets large and the main beam divides into three parts. Therefore, without high-order-mode cavity, both the S-parameters and the radiation patterns deteriorated.

### B. $8 \times 8$ DUAL LINEARLY POLARIZED ARRAY ANTENNA

To achieve higher gain for reliable high-speed data transmission, an  $8 \times 8$  dual LP antenna array is designed. Detailed configuration and size are shown in Fig. 8 and Table 3, respectively. For verification purpose, its corresponding antenna prototype is also fabricated as shown in Fig. 9. As the

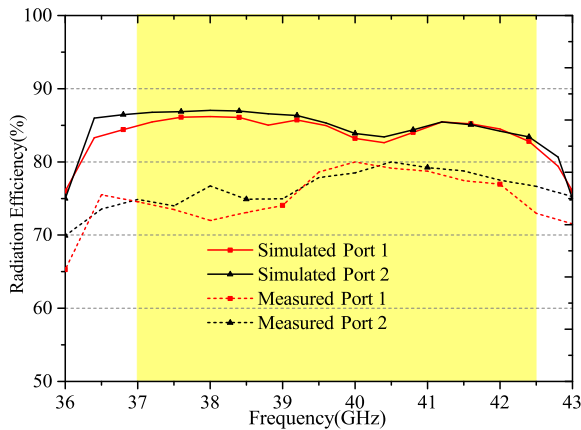


**FIGURE 13.** Simulated and measured radiation patterns of the  $8 \times 8$  dual LP antenna array at 37 and 42.5 GHz for both ports.

antenna array has a multi-layered geometry, the possible air gap between the PCB substrates may affect the characteristics of the fabricated prototype. To solve this problem, four screws arranged in each corner of the stacked substrates are employed to reduce the side effect of the air gap. In addition, during the fabrication process, the feeding networks are precisely aimed at the radiating ME-dipole radiators, which can further reduce transmission loss.

From bottom to top, the proposed  $8 \times 8$  antenna array are comprised of two vertically arranged modified H-shaped feeding networks in substrates 3 and 4 (as shown in Figs. 8(c) and 8(d)),  $4 \times 4$  high-order-mode cavities in

substrate 2 (as shown in Fig. 8(b)) and  $8 \times 8$  cavity-backed ME-dipole antenna array in substrate 1 (as shown in Fig. 8(a)), respectively. For low cost and stability considerations, the four substrates with each-layer 0.787 mm thick are stacked to form the proposed antenna array, as shown in Fig. 8(e).

In order to provide 1-to-4-way equal power allocation, each H-shaped power divider consists of two-level T-junction SIW feeding networks that are shown in Figs. 8(c) and 8(d). Because of phase difference of  $180^\circ$  between the four high-order cavities in row 1 and the ones in row 2 (it is similar between row 3 and row 4), the phase of feed ports in the lower row needs to fall behind that in the upper row by the same  $180^\circ$ . Here, by the adding the length of the SIW of the lower row (for example,  $F_{l2}$  is longer than  $F_{l1}$ ), all the antenna elements are fed by the same phase and uniform amplitude, resulting in uniform radiation and high gain. For a perfect T-junction (1-to-2-way power divider), the S-parameters of each output (P1 and P2 (as shown in Fig. 10(a))) should be larger than  $-3.5$  dB and nearly identical [19].

Fig. 10(a) shows that  $|S_{11}|$  is below  $-18$  dB in the desired frequency bands, while both  $|S_{12}|$  and  $|S_{13}|$  are larger than  $-3.5$  dB and almost the same. As shown in Fig. 10(b), the phase difference between output ports (P2 and P3) increases with the increase of difference value ( $F_{l2} - F_{l1}$ ). When the difference value ( $F_{l2} - F_{l1}$ ) is equal to 3.25 mm, the phase difference between output ports falls within  $180 \pm 18^\circ$ , which is acceptable for engineering applications.

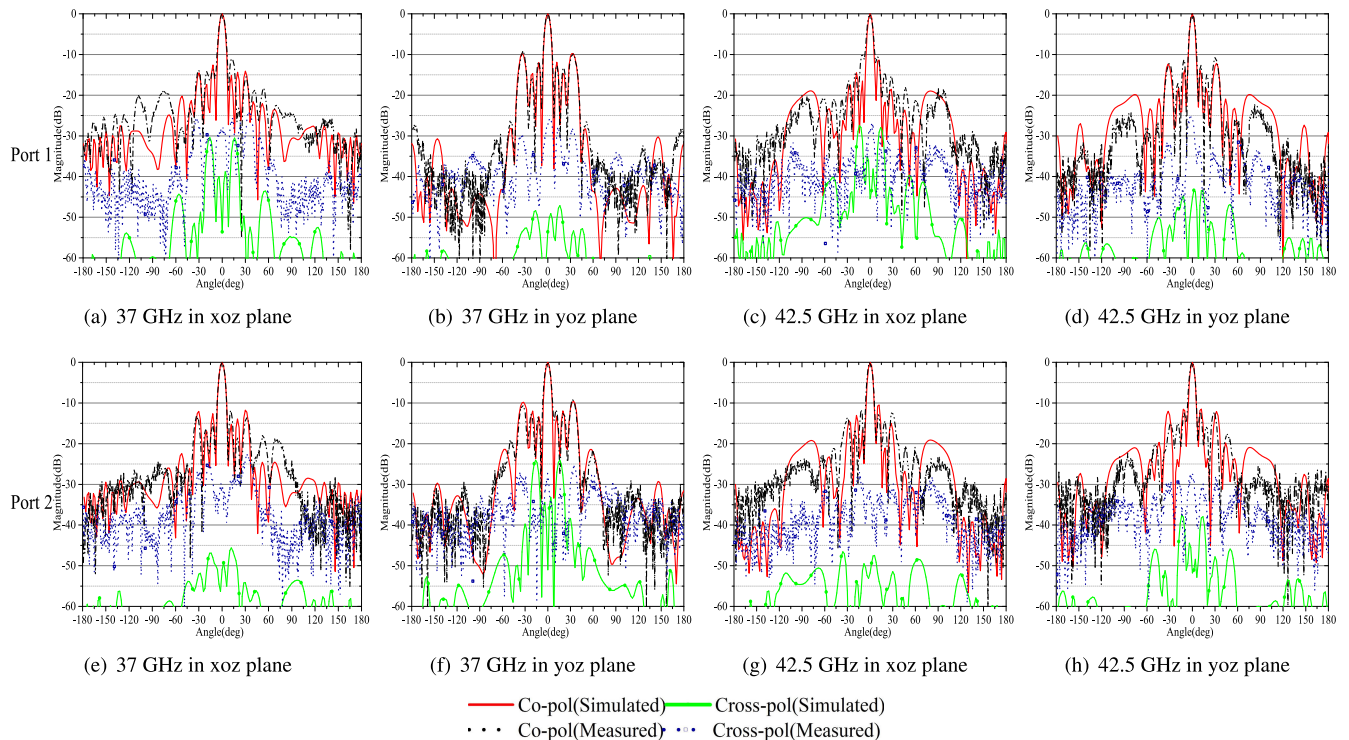


**FIGURE 14.** Radiation efficiency of the  $8 \times 8$  dual LP antenna array.

TABLE 4. Radiation performance of the 8 × 8 dual LP antenna array at different frequencies.

Parameter	Port 1								Port 2							
	XOZ-plane				YOZ-plane				XOZ-plane				YOZ-plane			
Frequency (GHz)	HPBW (deg)	Sidelobe (dB)	X-pol (dB)	FBR (dB)	HPBW (deg)	Sidelobe (dB)	X-pol (dB)	FBR (dB)	HPBW (deg)	Sidelobe (dB)	X-pol (dB)	FBR (dB)	HPBW (deg)	Sidelobe (dB)	X-pol (dB)	FBR (dB)
37 (Simulated)	7.4	-12.5	-30.4	31.8	7.5	-9.7	-47	30.4	7.4	-11.8	-45.6	31.5	7.5	-9.5	-24	31.5
37 (Measured)	7.6	-11.1	-25.7	31.6	7.6	-9.1	-26	28.3	7.4	-11.7	-22.3	32	7.6	-9.2	-25.2	30.1
42.5 (Simulated)	7.2	-11.3	-28.5	29.1	6.9	-12.1	-43.4	29.1	6.8	-10.4	-47.3	28.6	6.8	-12.1	-39	28.6
42.5 (Measured)	7.3	-9.5	-28	31.2	7	-10.7	-25	30.8	6.9	-11.6	-23.1	31.3	6.8	-12	-27.5	28.5

TABLE 5. Characteristics and performances comparison of proposed antenna array with other referenced antennas.

Refs.	Antenna type	Element Numbers	Im BW (Relative BW /GHz)	3-dB AR BW (Relative BW /GHz)	Peak gain (dBi/dBic)	Isolation (dB)	Dimension (mm <sup>3</sup> /λ <sub>0</sub> <sup>3</sup> )	Polarization	Remarks
Proposed LP array	High-order mode antenna	8 × 8	14.6% 36.8-42.6	N.A.	25.8	45	61.5 × 61.5 × 3.148 7.59 × 7.59 × 0.39	Dual LP	Wide bandwidth; High gain; High isolation; Dual polarization.
[10]	High-order mode antenna	2 × 2	3.8%(20.8-21.6) 2.7%(25.6-26.3)	N.A.	17.4	N.A.	31 × 31 × 2.4 6 × 6 × 0.48	LP	Low cost; Dual band; Single polarization.
[20]	Aperture-coupled patch Antenna	4 × 4	16.1% 56-63.1	N.A.	21.4	N.A.	30 × 30 × 2.4 6 × 6 × 0.48	LP	Wide bandwidth; High gain; Single polarization.
[21]	Cavity-backed slot Antenna	8 × 8	17.1% 55.7-66.1	N.A.	22.3	34.7	27 × 27 × 2.5 5 × 5 × 0.46	Dual LP	Wide bandwidth; High gain; Dual polarization.
[22]	Aperture-coupled patch antenna	2 × 2	18.2% 55-66	18.2% 55-66	17.85	15	70 × 100 × 0.787 12.8 × 18.4 × 0.14	Dual CP	Wideband; High gain; Dual polarization.

where λ<sub>0</sub>, LP, CP, N.A., AR BW, Im BW denote the free-space wavelength at the starting frequency, linear polarization, circular polarization, not available, axial ratio bandwidth, impedance bandwidth, respectively.

As shown in Fig. 11(a), a rectangular notch ( $W_{r1} \times L_{r1}$ , in yellow) is etched on the bottom of the substrate for each input port of the whole feeding network. It is used for inserting an input waveguide, namely, WR-22, whose working frequency band ranges from 33 to 50.1 GHz. Notably, by moving the vias in the middle connective band (in red), the widths of wide wall surrounding each input port (i.e., port 1) and each output port (i.e., port 2) are wider than the transmission waveguide, which helps to obtain good impedance matching. When input Port 1 is excited, nearly identical power can be achieved by the output Port 2. In other words, it is a low loss metallic waveguide to SIW transition. With the output port of this transition, the energy is further transmitted to the other output ports of the H-shaped network. Fig. 11(b) shows that across the desired frequency bands,  $|S_{11}|$  is less than -20 dB whereas  $|S_{12}|$  is nearly equal to 0, which further verifies the wideband and low transmission loss characteristics of the transition.

Fig. 12 shows the key performance parameters of the 8 × 8 dual LP antenna array. As observed in Fig. 12(a), the simulated and measured overlapped bandwidths are 15.8% (36.7 GHz-43 GHz) and 14.6% (36.8 GHz-42.6 GHz), respectively. Their corresponding gains are  $24.17 \pm 1.75$  dBi and  $23.8 \pm 2$  dBi, respectively, within the respective overlapped frequency bands. The measured bandwidth is narrower than the simulated one by 0.5 GHz, whereas the

measured gain is slightly lower than the simulated one by 0.37 dBi. Both of them can cover the desired frequency bands, and their corresponding gains are high enough for reliable data transmission. Fig. 12(b) shows that the simulated and measured  $|S_{21}|$  are less than -46.6 dB and -45 dB over the desired frequency bands, respectively, which exhibit low mutual coupling and strong anti-interference abilities for both input ports.

As an important parameter for power conversion rate, radiation efficiency of the 8 × 8 dual LP antenna array is shown in Fig. 14. The simulated radiation efficiencies for both ports are larger than 85%, whereas the corresponding measured ones are beyond 72%. The difference is mainly caused by the fabrication error and connecting cable loss. However, their curve trends are nearly the same. For a mm-wave antenna, radiation efficiency larger than 65% can meet the demand of practical applications.

Fig. 13 and Table 4 show the simulated and measured radiation patterns and characteristics of the 8 × 8 dual LP antenna array at 37 and 42.5 GHz for both ports. As displayed, for Port 1 at 37 GHz, the simulated HPBW, sidelobe level, X-pol level and FBR are 7.4°, -12.5 dB, -30.4 dB and 31.8 dB in XOZ-plane, respectively, and they are 7.5°, -9.7 dB, -47 dB and 30.4 dB in YOZ-plane, respectively. In comparison, the measured ones are 7.6°, -11.1 dB, -25.7 dB and 31.6 dB in XOZ-plane, respectively, and they are 7.6°,



−9.1 dB, −26 dB and 28.3 dB in YOZ-plane, respectively. At the upper frequency of 42.5 GHz, the simulated values are 7.2°, −11.3 dB, −28.5 dB and 29.1 dB in XOZ-plane, respectively, and they are 6.9°, −12.1 dB, −43.4 dB and 29.1 dB in YOZ-plane, respectively. Correspondingly, the measured ones are 7.3°, −9.5 dB, −28 dB and 31.2 dB in XOZ-plane, respectively, and they are 7°, −10.7 dB, −25 dB and 30.8 dB in YOZ-plane, respectively. The results of Port 2 nearly mirror that of Port 1 due to the nearly symmetrical structure. In total, the measured results well comply with the simulated ones, and they show low X-pol level, high FBR, narrow HPBW and reasonable sidelobe level.

### III. DISCUSSION AND COMPARISON

The main characteristics and performances of the proposed antenna array are compared with other referenced antennas, as shown in Table 5. In comparison, the proposed 8 × 8 LP antenna array has exhibited high gain and high isolation in a wide frequency band. Although the size (7.59 × 7.59 × 0.39λ<sub>0</sub><sup>3</sup>) is slightly larger due to the multi-layer ME-dipole structure, its practical dimensions of 61.5 × 61.5 × 3.148 mm<sup>3</sup> are still acceptable for an 8 × 8 unidirectional dual LP antenna array. As discussed above, the proposed antenna array with these characteristics may satisfy the needs of reliable high-speed data transmission and strong anti-interference ability in 5G mm-wave communication scenarios.

### IV. CONCLUSION

A dual LP high-order-mode mm-wave antenna with high gain and high isolation is proposed in this paper. A high-order-mode cavity with TM<sub>430</sub> mode is employed to excite a 2 × 2 slot-fed ME-dipole antenna subarray, resulting in high gain and wide bandwidth. Particularly, the high-order-mode cavity is fed by two vertically arranged slotted SIW feeding networks for double capacity, high isolation and low transmission loss. To further achieve high gain, an 8 × 8 antenna array fed by a pair of compact modified H-shaped full-corporate SIW networks is proposed. The working principles of the high-order-mode cavity and the feeding networks are also studied. Compared with the previously proposed dual-polarized mm-wave antennas, the proposed 8 × 8 antenna array can achieve both high gain (25.8 dBi) and high isolation (45 dB) in a wide frequency band (36.8–42.6 GHz) by using a low cost and low loss structure, and thus are applicable to the tough 5G communication scenarios with reliable high-speed data transmission and strong anti-interference ability.

### REFERENCES

- [1] World Radiocommunication Conference Allocates Spectrum for Future Innovation. Accessed: Nov. 27, 2015. [Online]. Available: [http://www.itu.int/net/pressofice/press\\_releases/2015/56.asp](http://www.itu.int/net/pressofice/press_releases/2015/56.asp)
- [2] Chinese Ministry of Industry and Information Technology Approved the New 5G Technology Test Frequencies. Accessed: Feb. 26, 2020. [Online]. Available: <http://www.miit.gov.cn/n1146290/n1146402/n1146440/c5730538/content.html>
- [3] B. Feng, L. Li, J.-C. Cheng, and C.-Y.-D. Sim, "A dual-band dual-polarized stacked microstrip antenna with high-isolation and band-notch characteristics for 5G microcell communications," *IEEE Trans. Antennas Propag.*, vol. 67, no. 7, pp. 4506–4516, Jul. 2019.
- [4] J. Zhu, S. Li, S. Liao, Y. Yang, and H. Zhu, "60 GHz Substrate-Integrated-Waveguide-Fed patch antenna array with quadri-polarization," *IEEE Trans. Antennas Propag.*, vol. 66, no. 12, pp. 7406–7411, Dec. 2018.
- [5] Y. Li and K.-M. Luk, "Low-cost high-gain and broadband Substrate-Integrated-Waveguide-Fed patch antenna array for 60-GHz band," *IEEE Trans. Antennas Propag.*, vol. 62, no. 11, pp. 5531–5538, Nov. 2014.
- [6] J. Zhu, C.-H. Chu, L. Deng, C. Zhang, Y. Yang, and S. Li, "Mm-wave high gain cavity-backed aperture-coupled patch antenna array," *IEEE Access*, vol. 6, pp. 44050–44058, 2018.
- [7] M. Asaadi, I. Affifi, and A.-R. Sebak, "High gain and wideband high dense dielectric patch antenna using FSS superstrate for millimeter-wave applications," *IEEE Access*, vol. 6, pp. 38243–38250, 2018.
- [8] A. Dadgarpour, B. Zarghooni, B. S. Virdee, and T. A. Denidni, "Millimeter-wave high-gain SIW end-fire bow-tie antenna," *IEEE Trans. Antennas Propag.*, vol. 63, no. 5, pp. 2337–2342, May 2015.
- [9] W. Han, F. Yang, J. Ouyang, and P. Yang, "Low-cost wideband and high-gain slotted cavity antenna using high-order modes for millimeter-wave application," *IEEE Trans. Antennas Propag.*, vol. 63, no. 11, pp. 4624–4631, Nov. 2015.
- [10] W. Li, K. D. Xu, X. Tang, Y. Yang, Y. Liu, and Q. H. Liu, "Substrate integrated waveguide cavity-backed slot array antenna using high-order radiation modes for dual-band applications in K - Band," *IEEE Trans. Antennas Propag.*, vol. 65, no. 9, pp. 4556–4565, Sep. 2017.
- [11] P. Wu, S. Liao, and Q. Xue, "A substrate integrated slot antenna array using simplified feeding network based on higher order cavity modes," *IEEE Trans. Antennas Propag.*, vol. 64, no. 1, pp. 126–135, Jan. 2016.
- [12] W. Yang, S. Chen, W. Che, Q. Xue, and Q. Meng, "Compact high-gain metasurface antenna arrays based on higher-mode SIW cavities," *IEEE Trans. Antennas Propag.*, vol. 66, no. 9, pp. 4918–4923, Sep. 2018.
- [13] T. H. Jang, H. Y. Kim, D. M. Kang, S. H. Kim, and C. S. Park, "60 GHz low-profile, wideband dual-polarized U-Slot coupled patch antenna with high isolation," *IEEE Trans. Antennas Propag.*, vol. 67, no. 7, pp. 4453–4462, Jul. 2019.
- [14] B. B. Adela, M. C. van Beurden, P. Van Zeijl, and A. B. Smolders, "High-isolation array antenna integration for single-chip millimeter-wave FMCW radar," *IEEE Trans. Antennas Propag.*, vol. 66, no. 10, pp. 5214–5223, Oct. 2018.
- [15] J. F. Zhang, Y. J. Cheng, Y. R. Ding, and C. X. Bai, "A dual-band shared-aperture antenna with large frequency ratio, high aperture reuse efficiency, and high channel isolation," *IEEE Trans. Antennas Propag.*, vol. 67, no. 2, pp. 853–860, Feb. 2019.
- [16] Y. Li and K.-M. Luk, "60-GHz dual-polarized two-dimensional switch-beam wideband antenna array of aperture-coupled magneto-electric dipoles," *IEEE Trans. Antennas Propag.*, vol. 64, no. 2, pp. 554–563, Feb. 2016.
- [17] W. X. An, H. Wong, K. L. Lau, S. F. Li, and Q. Xue, "Design of broadband dual-band dipole for base station antenna," *IEEE Trans. Antennas Propag.*, vol. 60, no. 3, pp. 1592–1595, Mar. 2012.
- [18] F. Xu and K. Wu, "Guided-wave and leakage characteristics of substrate integrated waveguide," *IEEE Trans. Microw. Theory Techn.*, vol. 53, no. 1, pp. 66–73, Jan. 2005.
- [19] Y. T. Lo and S. Lee, *Antenna Handbook: Theory, Applications, and Design*. New York, NY, USA: Springer, 2013.
- [20] J. Zhu, S. Liao, S. Li, and Q. Xue, "60 GHz wideband high-gain circularly polarized antenna array with substrate integrated cavity excitation," *IEEE Antennas Wireless Propag. Lett.*, vol. 17, no. 5, pp. 751–755, May 2018.
- [21] Z. Chen, H. Liu, J. Yu, and X. Chen, "High gain, broadband and dual-polarized substrate integrated waveguide cavity-backed slot antenna array for 60 GHz band," *IEEE Access*, vol. 6, pp. 31012–31022, 2018.
- [22] J. Zhu, S. Liao, Y. Yang, S. Li, and Q. Xue, "60 GHz dual-circularly polarized planar aperture antenna and array," *IEEE Trans. Antennas Propag.*, vol. 66, no. 2, pp. 1014–1019, Feb. 2018.



**BOTAO FENG** (Senior Member, IEEE) was born in Guangdong, China, in 1980. He received the B.S. and M.S. degrees in communication engineering from the Chongqing University of Posts and Telecommunications (CQUPT), Chongqing, China, in 2004 and 2009, respectively, and the Ph.D. degree in communication and information system from the Beijing University of Posts and Telecommunications (BUPT), Beijing, China, in 2015.

He joined Nokia Mobile Phones Ltd., Dongguan, China, as a Communication Engineer, in 2004. From 2009 to 2012, he was a Senior Engineer and a Chief Executive with China United Network Communications Company Ltd., Guangdong. Since February 2020, he has been an Adjunct Senior Research Fellow with the Energy Materials Telecommunications (EMT) Research Centre, Institut national de la recherche scientifique (INRS), Canada. He is currently a Full-Time Postgraduate Advisor and a Postdoctoral Advisor with Shenzhen University, China, where he is also the Head of the Laboratory of Wireless Communication, Antennas and Propagation and the Deputy Director of the Department of Electronic Science and Technology. He is specially invited as the Chief Scientist with Shenzhen Nandouxing Technology Company Ltd. He is the President of Shenzhen Taobida Technology Company Ltd., and so on. He has authored or coauthored more than 50 Science Citation Index (SCI)- and Engineering Index (EI)- articles. He holds over 20 invention patents. He and his research team members are currently conducting over ten projects on antenna development and design for 5G/THz and future communications, which are supported by the natural science research funds and industrial cooperation research and development funds. His several antenna designs for 5G applications have been widely used with the Chinese communication operators. It is estimated that the related total production value is approximately 200 million Ren Min Bi (RMB). His research interests include antennas and mobile communications and so on.

Dr. Feng serves concurrently as a Senior Evaluation Experts for the Degree and Graduate Education Center, Chinese Ministry of Education, the Natural Science Foundation Committee of Guangdong Province, the Information and Communication Technologies Senior Title Evaluation Committee of Guangdong Province, and the Science and Technology Innovation Committee of Shenzhen City, and so on. He received the Award of Breakout Star of the Year and the title of Technical Innovation Expert. In 2017, he received the Award of the Outstanding Instructor (First Prize) with the National Graduate Electronic Contest, the Tencent Outstanding Teacher Award, and so on. He serves as a Regular Peer Reviewer, a Technical Committee Member, a Section Chair, and a Guest Editor for the IEEE/IET, Elsevier, Wiley, and Springer journals and conferences on microwave technique and antenna development.



**YATING TU** was born in Zhanjiang, Guangdong, China, in 1994. She received the B.S. degree from Shenzhen University, in 2017, where she is currently pursuing the M.S. degree. Her research interests include design of wideband antenna, base-station antenna, reconfigurable antenna, and so on. She received the Best Paper Award, in 2019, the International Workshop on Electromagnetics, Applications and Student Innovation Competition (IWEM 2019).



**JUNLONG CHEN** was born in Guangxi, China, in 1996. He received the B.S. degree from the Guilin University of Electronic Technology, in 2018. He is currently pursuing the M.S. degree with Shenzhen University, China. His research interests include base-station antenna, millimetre-wave antenna, and so on. He was one of the winners for the presentation prize with the 2019 International Workshop on Electromagnetics, Applications and Student Innovation Competition (IWEM 2019).



**SIXING YIN** (Member, IEEE) received the B.S., M.S., and Ph.D. degrees from the Department of Information and Communication Engineering, Beijing University of Posts and Telecommunications, China, in 2003, 2006, and 2010, respectively. He was a Visiting Scholar with The Hong Kong University of Science and Technology, in 2009. He was a Postdoctoral Fellow with the Beijing University of Posts and Telecommunications, from 2010 to 2012. He is currently an Associate Professor with the School of Information and Communication Engineering, Beijing University of Posts and Telecommunications, and a Visiting Scholar with Carleton University. His research interests include system design and machine-learning-inspired technologies in wireless communications.

He is currently an Associate Professor with the School of Information and Communication Engineering, Beijing University of Posts and Telecommunications, and a Visiting Scholar with Carleton University. His research interests include system design and machine-learning-inspired technologies in wireless communications.



**KWOK L. CHUNG** (Senior Member, IEEE) received the B.E. (Hons.) and Ph.D. degrees in electrical engineering from the University of Technology Sydney, Australia, in 1999 and 2005, respectively. He joined the Faculty of Engineering, University of Technology Sydney, in 2004, as a Lecturer. In 2006, he joined The Hong Kong Polytechnic University, where he spent about six years with the teaching of electronic and information engineering. In 2012, he joined the Institute

for Infrastructure Engineering, Western Sydney University, as a Research Fellow. In 2015, he joined the Qingdao University of Technology (QUT), China, as a Cross-Disciplinary Research Professor and a Supervisor of Ph.D. students. He is currently the Director of Civionics Research Laboratory where he leads a Cross-Disciplinary Research Team with QUT. He has authored or coauthored about 120 publications (SCI and EI) with various areas of electrical and civil engineering. His current research interests include passive wireless sensors for structural health monitoring, cement-based materials design and characterization, microwave antennas, and metasurface designs. He is a member of the International Steering Committee of the IEEE International Workshop on Electromagnetics (iWEM). He received the Award of the Outstanding Associate Editor with IEEE ACCESS, in 2018. He was the Vice Chair and the Chairman of the IEEE AP/MTT Hong Kong Joint Chapter, in 2010 and 2011, respectively. He is the Founding Chair and the Chair of the IEEE Qingdao AP/MTT/COM Joint Chapter (CN10879) under Beijing Section. He has been an Associate Editor of IEEE ACCESS, since 2016. He serves as a Reviewer for the numerous IEEE, IET, Elsevier, and other international journals.

...